River Flow 2010 - Dittrich, Koll, Aberle & Geisenhainer (eds) - © 2010 Bundesanstalt für Wasserbau ISBN 978-3-939230-00-7

Changes in Three-Dimensional Flow Structure at a River Confluence with Changes in Momentum Ratio

Shinjiro Miyawaki, George Constantinescu
Dept. of Civil and Environmental Engineering & IIHR-Hydroscience and Engineering, The University of Iowa, Iowa City,Iowa U.S.A.

Bruce Rhoads
Dept. of Geography, University of Illinois at Urbana-Chanpaign, Urbana, Illinois U.S.A.

Alexander Sukhodolov
Dept. of Ecohydrology, Institute of Freshwater Ecology and Inland Fisheries, Berlin, Germany

ABSTRACT: High-resolution eddy-resolving numerical simulations of the flow at an asymmetric river confluence with concordant bed are used to investigate the effect of the momentum ratio on the flow and turbulence structure. The focus is on a case with a value of the momentum ratio between the two streams close to five. To better understand the effect of the momentum ratio on the flow hydrodynamics, comparison is shown with results from a numerical simulation of the flow at the same confluence but with a momentum ratio close to one. The Detached Eddy Simulation (DES) solutions are used to investigate the changes in the dynamics of large-scale coherent structures, in particular, the mixing layer vortices and the streamwise oriented vortical cells forming on the sides of the mixing layer. The comparison between the two cases shows that: (1) the quasi two-dimensional vortices shed in the mixing layer change from wake type to vortex sheet type as the momentum ratio increases from one to five; the coherence of these eddies and their capacity to entrain sediment from the bed is much larger in the later case; (2) while being of comparable strength when the momentum ratio is close to one, the streamwise oriented cell on the high momentum side of the mixing layer is much stronger than the cell on the low-momentum side of this layer when the momentum ratio is large.

Keywords: Confluence, Detached Eddy Simulation, large scale coherent structures, mixing layer

1 INTRODUCTION

River confluences are fundamental elements of river networks. A significant change in the flow hydrodynamics (e.g., the formation of a mixing layer starting at the confluence apex), bed geometry, and water quality is generally observed for some distance downstream of the confluence. Interest in flow hydrodynamics and transport processes (sediment and contaminant transport, heat transfer), and their morphological and ecological implications (e.g., development of large scour holes, increase of aquatic habitat for some river organisms), has generated a considerable amount of research during the last few decades. Mosley (1976) conducted one of the first laboratory experiments to understand the main characteristics of flow and mixing at river junctions.

Field studies have been performed to investigate flow and turbulence structure at river confluences quantitatively by analyzing point measurement data (e.g., Rhoads and Sukhodolov, 2001, 2008; Sukhodolov and Rhoads, 2001). Other studies have focused on the relationship between the flow, turbulence and sediment transport (e.g., Boyer et al., 2006) because confluences play an important role in regulating the movement of sediment through river systems. The main advantage of field studies over laboratory studies is that they are free of scale effects.

Related laboratory and theoretical studies have been performed to quantitatively characterize the spatial development of shallow mixing layers developing in channels with flat beds. In most cases these investigations consider only the simplest case of a mixing layer developing between two parallel incoming streams (e.g., Chu et al., 1991). The direct relevance of these shallow mixing layer studies to river confluences, and especially for cases with a momentum ratio between the two streams that is close to unity, is limited. Field studies suggest that shallow mixing layers at confluences are complex (Rhoads and Sukhodolov, 2004) because the incoming streams generally are not parallel; scour holes develop downstream of the confluence; channel alignment downstream of

the confluence may be curved rather than straight, and quasi two-dimensional (2D) mixing-layer vortices can interact with streamwise-oriented vortices that may develop on one or both sides of the mixing layer. The mechanism responsible for the formation of these streamwise cells of helical motion was discussed, among others, by Rhoads (1996), Paola (1997) and Miyawaki et al., (2009). For confluences with a large angle between the incoming streams, these cells, rather than the predominantly vertical quasi-2D mixing layer vortices, play the most important role in the mixing and sediment entrainment that occurs in the confluence hydrodynamic zone (CHZ) (Kenworthy and Rhoads, 1995). For example, sediment particles entrained at the bed beneath streamwise-oriented helical cells can be convected over large distances inside the core of these cells before being ejected back into the surrounding turbulent flow. The cells act as a pumping mechanism for sediment over considerable distances downstream of the confluence apex and play a determinant role in the formation of the scour hole observed at most river confluences.

The complexities of the flow and transport processes in the confluence region are still to be fully understood. Field studies provide a powerful tool to investigate the flow, turbulence, mixing and sediment transport processes at river confluences. However, recent advances in the numerical simulation of complex turbulent flows at large (field) Reynolds numbers allow an alternative approach to investigate these flows. For example, Miyawaki et al. (2009) succeeded in reproducing the main features of the three-dimensional flow field at an asymmetrical river confluence with concordant bed using Detached Eddy Simulation (DES). Additionally, the mixing between the two streams was investigated by Miyawaki (2009). DES is a hybrid model that behaves like a Reynolds Averaged Navier-Stokes (RANS) model near the solid boundaries and like a Large Eddy Simulation (LES) model away from them. The switch to RANS in the near-wall regions allows simulations to be performed for Reynolds numbers typical of field settings using much less computational resources than those required by well-resolved LES.

Once validated, the advantage of such a fully 3D numerical model is that it provides the whole three-dimensional instantaneous and mean flow fields at a resolution that is much more detailed than the point sampling provided by field studies. Additionally, the distributions of the friction velocity and pressure root-mean-square (rms) fluctuations at the bed are available from these simulations. These two variables are hard to estimate accurately for natural channels, and in particular for river confluences. The data provided by a sufficiently well resolved DES illuminates details of the flow, turbulence structure and sediment erosion processes. Eddy resolving techniques also allow a detailed characterization of the type and scale of the dynamically important turbulent structures controlling the momentum and mass exchange processes in the CHZ. Of particular interest is to be able to characterize the position, spatial extent and the strength of the streamwise-oriented cells of helical motion forming on one or both sides of the mixing layer and the position and spatial growth of the mixing layer originating at the confluence apex.

The momentum ratio between the two incoming streams is known to be one of the key parameters that control the flow hydrodynamics and mixing in the CHZ. In the numerical simulation conducted by Miyawaki et al. (2009), the momentum ratio was close to unity. To understand the qualitative and quantitative changes in the flow structure with momentum ratio, a numerical simulation of field conditions with a high momentum ratio (~5) is conducted in the present study and compared to the simulation with a momentum ratio close to unity.

2 NUMERICAL SIMULATION

2.1 *Description of the test cases*

The study site is the confluence of the Kaskaskia River (KR) and the Copper Slough (CS) in east central Illinois, U.S.A. KR has sandy bed material (d_{50} = 0.67 mm), while CS has a mixed sand and gravel bed (d_{50} = 3.5 mm). The bathymetry and flow conditions at the confluence were measured in two field studies conducted by Rhoads and Sukhodolov (2001, 2008). The flow and geometrical parameters in the simulations are close to those in the experiments. In this paper, the simulation for field conditions in Rhoads and Sukhodolov (2001) is called Case 1 and the simulation for field conditions in Rhoads and Sukhodolov (2008) is called Case 2. The field measurements in Case 2 were obtained one year after those for Case 1.

Table 1 compares the flow conditions for the two test cases. The middle row in Table 1 contains variables calculated using the average values of the velocity and depth between the two streams. The momentum of a certain stream (i) is defined as $\rho Q_i U_i$, where Q_i and U_i are the discharge and mean velocity in the stream. The momentum ratio (Mr) between the two streams in Case 2 (Mr~5.4) is about five times larger than the one in Case1 (Mr~1), as CS has much more momentum

than KR. The other important difference between the flow conditions in the two test cases is that the mean flow depth in Case 2 is about two thirds that in Case 1. The physical Reynolds numbers (*Re*) based on the mean velocity and the mean flow depth in Case 1 and Case 2 are approximately 166,000 and 77,000, respectively.

The paper by Miyawaki et al. (2009) contains a validation study of Case 1 for which detailed field data were available at several cross sections. This paper focuses on comparing the flow and turbulence structure in Case 2 to those in Case1.

In the following discussion, all the quantities are non-dimensionalized using the mean velocity (U) and the mean depth (D) in Case 1, i.e., U = 0.45 m/s and D = 0.36 m (see also Table 1).

The cross-section of both tributaries is trapezoidal. The KR tributary is close to parallel to the downstream channel, while the CS tributary forms an angle of about 60^0 with the downstream channel. As can be seen from Fig. 1 in which the datum corresponds to the position of the free surface in Case 1 and the datum in Case 2 is situated at z`=0.58D, the maximum depth of the scour hole is about the same (~3.0D) in the two cases, but the volume of the scour hole in Case 2 is significantly smaller than that in Case 1. An important qualitative difference between the two bathymetries is that the shallow region, representing a submerged bar located between cross-sections A and C in Case 2, is not present in Case 1. On the CS side, the bank curvature at the entrance into the downstream channel is high.

2.2 *Numerical model*

A general description of the DES code is given in Chang et al. (2007). The 3-D incompressible Navier-Stokes equations are integrated using a fully implicit fractional-step method. The governing equations are transformed to generalized curvilinear coordinates on a non-staggered grid. The convective terms in the momentum equations are discretized using the fifth-order accurate upwind biased scheme. All other terms in the momentum and pressure-Poisson equations are approximated using second-order central differences. The discrete momentum (predictor step) and turbulence model equations are integrated in pseudo-time using alternate direction implicit (ADI) approximate factorization scheme. The Spalart-Allmaras (SA) one-equation model was used as the base model in DES. Time integration is done using a double time-stepping algorithm and local time stepping is

Table 1. Flow conditions in the two incoming streams (i=1 and i=2, respectively) and main non-dimensional parameters of the confluence flow in Case 1 and Case 2.

Case	Stream	Q_i (m^3/s)	U_i (m/s)	$\rho Q_i U_i$ (kg·m/s)	D_i (m)	*Re*	*Fr*	*Mr*
1	KR	1.41	0.42	597	0.48	166,000	0.24	1.0
			0.45		0.36			
	CS	1.34	0.46	615	0.32			
2	KR	0.35	0.19	65	0.28	77,000	0.22	5.4
			0.34		0.23			
	CS	0.75	0.45	337	0.19			

*KR = Kaskaskia River, CS = Copper Slough, *Mr* = Momentum ratio

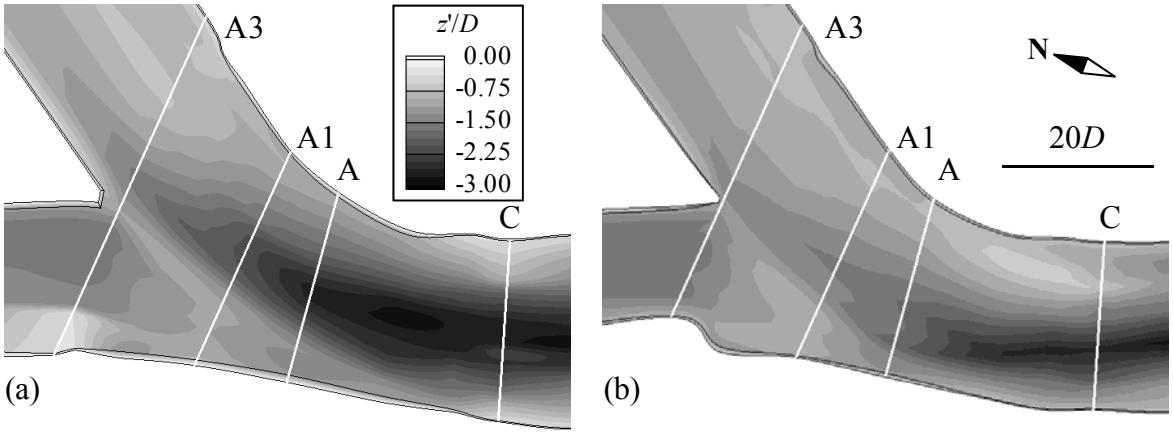

Figure 1. Bathymetry in the region surrounding the confluence. (a) Case 1, (b) Case 2. The bathymetry is visualized using non-dimensional bed elevation contours, z'/D.

used to accelerate the convergence at each physical time step. The time discretization is second order accurate. Miyawaki et al (2009) showed that DES predictions of the mean velocity fields are in very good agreement with the field measurements for Case 1. Additional river engineering applications using the same DES code and validation are discussed in Kirkil and Constantinescu (2009) and Koken and Constantinescu (2009).

2.3 *Simulation setup*

The simulation setup and boundary conditions for Case 2 are similar to those used for Case 1. The mean of the average depths and average velocities in the KR and CS streams are 0.23 m and 0.34 m/s, respectively, for Case 2. These two quantities can be used to define a physical Reynolds number for Case 2. Based also on information from the field study, the equivalent non-dimensional bed roughness is close to 170 wall units corresponding to a physical roughness height of 0.01 m. The channel bed and lateral walls are treated as rough no-slip boundaries.

At the two inflow sections, turbulent inflow conditions corresponding to fully-developed turbulent channel flow are applied. The velocity fields from preliminary periodic-channel LES simulations are stored in a file and then fed in a time-accurate manner through the two inflow sections, KR and CS.

At the outflow, a convective boundary condition is used. The free surface is treated as a rigid lid. This is justified, as, similar to Case 1, the channel Froude number in Case 2 is relatively small (Fr=0.22). The computational domain was meshed with about 5 million cells. The physical time step is close to 0.07 sec.

3 RESULTS

3.1 *Mixing layer vortices*

The DES results show that the axes of the mixing layer (ML) vortices remain close to vertical over the whole channel depth as they are convected downstream – a result consistent with the field data (Rhoads and Sukhodolov, 2008). Fig. 2 visualizes the mixing layer vortices in the two cases using instantaneous out-of-plane vorticity contours plotted on a surface situated 0.1D below the surface. The black patches contain high negative vorticity and correspond to the clockwise rotating vortices. The white patches contain high positive vorticity and correspond to the location of counter-clockwise rotating vortices.

As previously discussed, a shallow region exists in Case 2 between cross-sections A and C along the KR inner bank (see Fig. 1b). The flow depth is less than 0.1D over this submerged bar and thus the bar intersects the horizontal plane of vorticity contours (Fig. 2B). The bar changes the flow pattern dramatically compared to Case 1. As the flow from the CS tributary reaches the submerged bar, it forms relatively strong shear layers on both sides of this feature.

In Case 1, a shear layer marked by positive vorticity forms close to the CS side near the downstream junction corner (section A1) and extends outward into the main flow. The development of this shear layer is related to the abrupt change in alignment of the curved bank. Similar shear layers develop at the inner bank in open channel bends of high curvature (Zeng et al., 2008). In Case 2, the effect of the submerged bar shifts this shear layer close to the channel bank. The shear layer detaches from the inner (CS) bank of the downstream channel and diverges around the bar between sections A and C, with the strongest limb on the left side of the submerged bar. Thus, as opposed to Case 1 in which the near-

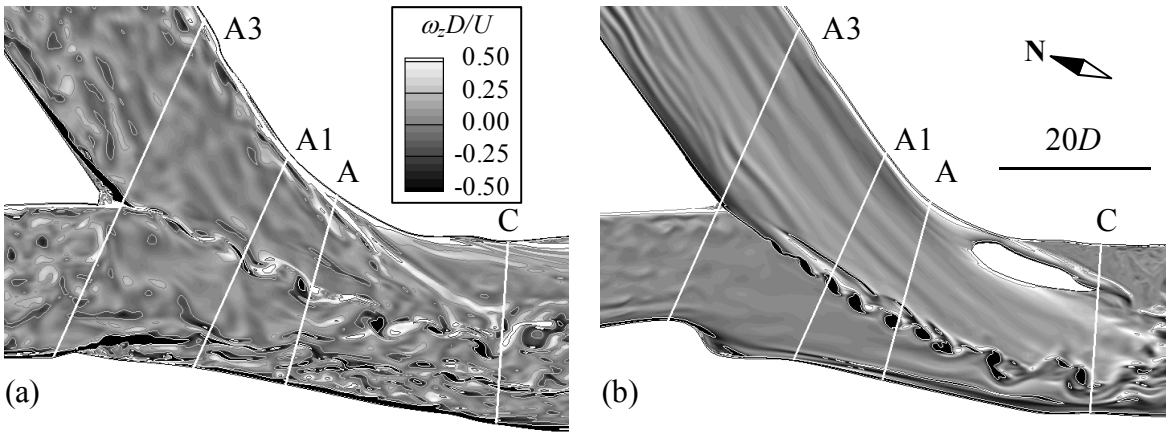

Figure 2. Visualization of the vortical structure of the flow in a horizontal plane situated 0.1D below the free surface using non-dimensional out-of-plane (vertical) vorticity contours. (a) Case 1, (b) Case 2.

bank shear layer extends outward to interact with the downstream part of the ML (around section C), in Case 2 the inner-bank shear layer does not affect the downstream development of the ML. Also in Case 2, a large recirculation region forms downstream of section C on the CS side of the channel. Such a recirculation region is not present in Case 1. Its formation has important consequences for the mixing processes and sediment transport and deposition in the main channel.

Another difference observed in the vorticity distributions shown in Figs. 2a and 2b is the absence of large-scale energetic eddies on the KS side of the channel. These eddies are generated in Case 1 because of the presence of a submerged block of sediment near section A3 that formed due to bank failure. A strong mixing layer forms as water is pushed over the top of the block of sediment. The water depth is not large enough in Case 2 to submerge the block of failed material. Thus, the main mechanism responsible for the generation of the strong eddies close to the KS bank is not present in Case 2.

The structure of the ML is very different in the two cases. As shown in Fig. 2, the ML contains only clockwise-rotating vortices in Case 2, whereas an array of alternating clockwise and counter-clockwise rotating vortices is observed in Case1. This qualitative difference in the structure of the ML is not a consequence of the difference in the bathymetry in the two cases. Rather, it is directly related to the relative differences in the mean streamwise velocities and streamwise momentums between the two streams.

The formation of the ML vortices in Case 2 is mainly driven by the growth of the Kelvin-Helmholtz instability that develops between two streams of different velocity (vortex sheet type). In Case 1, the formation of the ML vortices is mainly driven by the interaction of the detached shear layers forming on the two sides of the confluence apex. The mixing layer vortices in Case 1 resemble the von Karman vortex street developing behind a bluff body (wake type). The wake recirculation region is negligible in Case 2, as the shear layers remain attached until very close to the confluence apex. By contrast, in Case 1 the shear layers detach some short distance upstream of the confluence apex and the interaction of their downstream ends induces the alternate shedding of eddies containing positive and negative vorticity, similar to the case of flow past a bluff body. Because the mean velocity on the CS side in Case 1 is slightly larger (by about 10%) than the mean velocity on the KS side, the clockwise-rotating vortices are, on average, slightly stronger (e.g., larger circulation, more compact distribution of the vorticity within the core of the vortex) than the counter-clockwise rotating ones. In Case 2, no counter-clockwise rotating vortices are observed over the upstream part of the mixing layer. The white streak of negative vorticity present on the CS side of the ML is due to the fact that the horizontal plane cuts through the strong streamwise oriented vortex forming on the CS side of the ML. This interaction explains the formation of patches of positive vorticity on the CS side of the ML farther downstream (sections A-C).

The large horizontal shear present in Case 2 is responsible for the formation of a ML of vortex sheet type. The small horizontal shear present in Case 1 means the vortex sheet type is still present. However, the structure and dynamics of the shear layers developing on both sides of the confluence apex and the ML vortices show that the ML in Case 1 is dominantly of wake type.

Even in cases when the difference in the mean streamwise velocity between the two streams is small (e.g., Case 1, see Table 1), a well defined ML-like region forms at confluences if the angle between the two tributaries is not equal to zero. In these cases, the usual definition of the mixing layer thickness as the maximum slope thickness at a certain section will predict a negligible thickness of the mixing layer, which is wrong. In this paper, we will define the ML thickness as the width of the region in which the ML vortices are convected downstream. As expected, the width of this region increases downstream, at least until the ML approaches one of the banks (e.g., the KS bank in Case 2), or it starts interacting with large-scale eddies generated by other flow and bathymetric features (e.g., the eddies generated by the passage of the flow over the submerged bank block near section A3 in Case 1). As inferred from Fig. 2, the ML thickness at cross-section A in Case 2 is approximately half the one in Case 1. Despite the fact that the ML is thicker in Case 1, the coherence of the clockwise rotating ML vortices is larger in Case 2. The dominant frequency of passage of the vortices at cross-section A1 is about $0.20U/D$ for Case 2 and $0.15U/D$ for Case 1. The frequency for case 2 is nearly identical with the frequency obtained from the field data (Rhoads and Sukhodolov, 2008).

Compared to Case 1, where the ML remains close to the channel centerline, the ML shifts strongly toward the KR side in Case 2. This is obviously due to the large difference in the momentum ratio between the two streams and the presence of the very shallow region close to the CS side that diverts the flow toward the opposite bank of the downstream channel. The difference in the mean channel depths is expected to play a relatively minor role in the shift of the ML. Again the

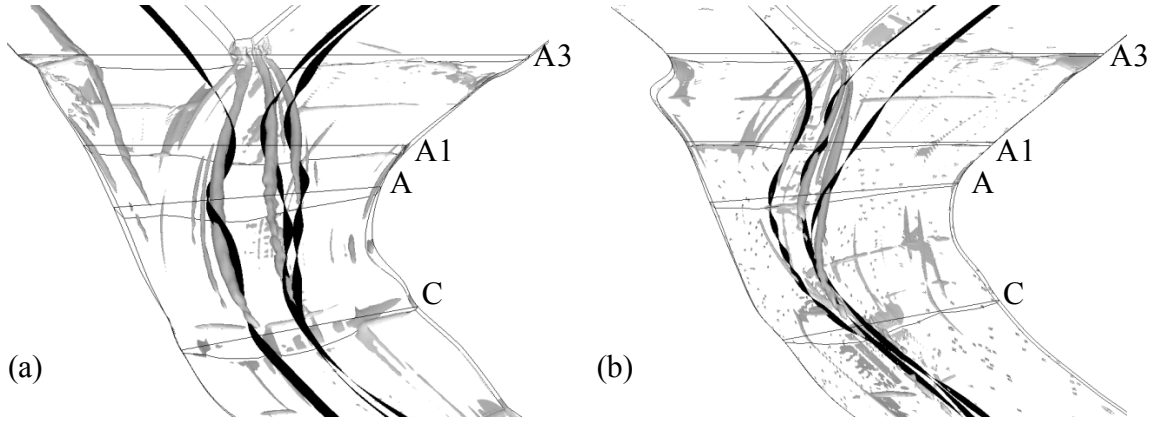

Figure 3. Visualization of the vortical structure of the flow using the Q-criterion; the Q=0.05$(U/D)^2$ iso-surface is shown. (a) Case 1, (b) Case 2.

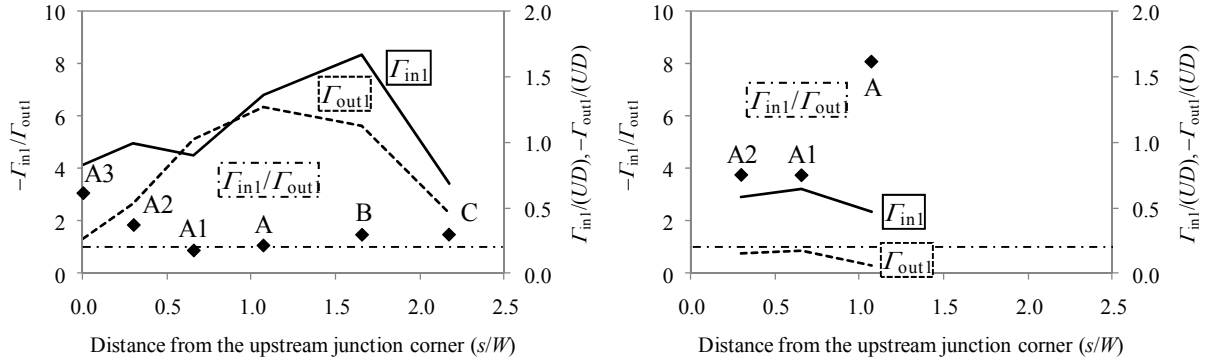

Figure 4. Streamwise variation of the non-dimensional circulation of the two streamwise-oriented vortices and of the ratio between the circulations of the two vortices. (a) Case 1, (b) Case 2. The dash dotted line shows the level corresponding to $\Gamma_{in1}/\Gamma_{out1}$=1

simulation results conform with field data (Rhoads and Sukhodolov, 2001, 2008).

3.2 *Streamwise-oriented vortices*

It is well known that the ML vortices drive the momentum and mass exchange in the cross-stream direction in a shallow mixing layer if the tributaries are parallel (e.g., Uijttewaal and Booij, 2000). The situation changes dramatically in the case when the angle between the two tributaries is large and the relative difference between the momentums of the two tributaries is small. This is because strong streamwise-oriented vortices (SVs) form on one or both sides of the mixing layer (Rhoads and Kenworthy, 1995; Rhoads and Sukhodolov, 2008). For example, Miyawaki (2009) has shown that in Case 1 the mixing of mass in the cross-stream direction is mainly driven by the SVs rather than the ML vortices. If the angle between the two tributaries is large and the relative difference between the momentums of the two tributaries is also large, one expects both the ML vortices and the streamwise oriented cells to play an important role in the momentum and mass exchange at the confluence. Case 2 offers a good illustration of this situation. The relative roles of different types of large-scale eddies in mixing depends on the exact values of the momentum ratio, confluence angle, orientation of the incoming streams, channel curvature and the bathymetry in the confluence region.

DES allows a quantitative comparison of the position, extent and strength of the SVs. Figure 3 visualizes the position of the SVs in the mean flow using the Q-criterion. Additionally, several 3-D ribbons were added to show the direction of the flow within the SVs and visualize the helical motions followed by the particles inside the SVs.

In both cases, two SVs are present on the CS side of the ML (the one which is situated the closest to the ML is denoted SV_{in1}, the other is denoted SV_{in2}) and one SV is located on the KR side of the ML (SV_{out1}). Consistent with the mechanism responsible for the formation of the SVs which induces a vertical flow component toward the bed within the mixing layer (Rhoads, 1996), the direction of the rotation of the two SV_{in} vortices is opposite to that of SV_{out}.

Fig. 3 also shows that in Case 1 SV_{in1} is much stronger at all cross sections than SV_{in2}. This is expected to happen in most cases, at least over the upstream part of the ML where the two incoming streams come in contact. The formation of the secondary cell SV_{in2} is directly induced by that of the primary cell SV_{in1}. In Case 2, the differences between the circulations of the two cells are much smaller. Still, analysis of the simulation results

shows the circulation of SV_{in1} is larger than that of SV_{in2} over the upstream part of the ML. Moreover, the circulation of SV_{in2} becomes larger than the one of SV_{in1} downstream of section A. The two vortices also start exchanging vorticity. This has obviously to do with the presence of the submerged bar which diverts the flow on the CS side toward the downstream part of the ML. This primarily enhances the strength of the vortex that first is affected by the diverted flow (SV_{in2}). Another obvious qualitative difference between the two cases is the small size of SV_{out} in Case 2. In Case 2, the momentum of the CS stream is about five times that of the KR stream. This imbalance pushes the ML toward the KR side and creates the conditions for the formation of a stronger SV on the CS side than on the KR side. As a result, the SV on the low momentum (KS) side is very weak.

Figure 4 shows the streamwise variation of the non-dimensional circulation of SV_{in1} and SV_{out1} in the two cases. At cross-section A1 situated at $s = 0.66W$ (s is the streamwise distance measured from the apex, W is the average width of the downstream channel) the circulation of SV_{in1} is about four times that of SV_{out1} in Case 2, while they are almost the same in Case 1 (as shown in Fig. 4a, $-\Gamma_{in1}/\Gamma_{out1}\sim1$ downstream of section A1). As one moves downstream and the coherence of SV_{in1} is gradually lost, the ratio continues to increase (e.g., it is about 8 at section A). Despite the lower discharges in both streams and lower channel depth in Case 2 (both of these variables limit the capacity of the flow to form strong SVs), the circulation of SV_{in1} in Case 2 is comparable (two thirds at section A1) to that in Case 1. However, the circulation of SV_{out1} in Case 2 is only one sixth of that in Case 1.

3.3 *Friction velocity*

Although sediment transport was not simulated in this numerical simulation, the bed friction velocity distribution (see Fig. 5) is indicative of locations where sediment entrainment is likely to occur. The bed friction velocities in the CS stream are comparable in the two simulations as the mean streamwise velocities were similar. On the other hand, the values of u_τ/U in the KS stream are much larger in Case 1 because the mean velocity was about 2.5 times larger than in Case 2. Also, in Case 2 no region of strong amplification of u_τ/U is observed at the KR bank close to section A3 because the failed bank material was not submerged. The values of u_τ/U over the submerged bar are also small due to the shallow flow and low velocities in that portion of the confluence.

In both cases the largest values of u_τ/U are not associated with the fastest incoming stream (e.g., on the CS side in Case 2). Downstream of the confluence apex regions of high values of u_τ/U correspond to the locations of the SVs. Though the bed friction velocity is amplified beneath the ML, the amplification is lower than that beneath some of the SVs. This result shows that even for a confluence with a large difference in streamwise velocities and momentum fluxes between the two incoming streams, the SVs play a primary role in the growth of the scour hole. The importance the SVs is related to the high angle of the confluence, which promotes turning of the flows and the development of vorticity. Obviously, if the confluence angle decreases and the momentum ratio increases, eventually the ML vortices will induce larger values of u_τ/U compared to the SVs.

The maximum amplification of the bed friction velocity is observed underneath the SV_{in}s in Case 2. In Case 1 the maximum amplification is observed beneath the primary SV forming on both sides of the ML. This is expected given the variation of the coherence of the various SVs between Case 1 and Case 2 (see discussion of Fig. 4). More interestingly, the maximum friction velocity is about $0.15U$ in both cases, and the area containing

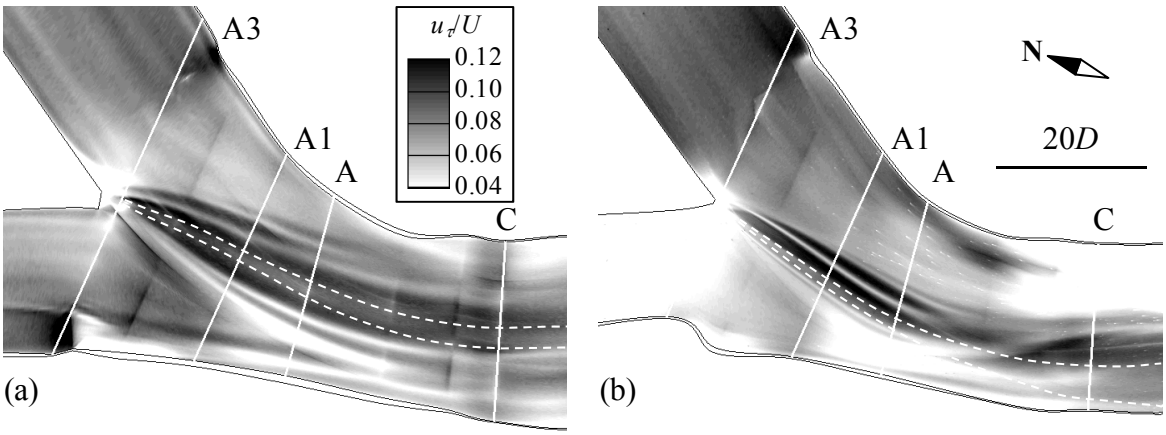

Figure 5. Distribution of the non-dimensional bed friction velocity, u_τ/U, in the mean flow. The dashed lines delimitate the extent of the mixing layer. (a) Case 1, (b) Case 2.

high values of u_*/U is slightly larger in Case 2 despite the fact that the circulation of the SVs is always larger in Case 1. The reason is that the flow is shallower in Case 2 and the cores of the SVs are situated closer to the bed surface.

4 CONCLUSIONS

DES simulations of flow at an asymmetric confluence were conducted to understand the effects of the momentum ratio on the flow structure and the capacity of the stream to entrain sediment from the bed in the confluence hydrodynamic zone. The simulation data were used to perform a detailed quantitative analysis of fluid turbulence, in particular the large-scale eddies that control mass and momentum transport in the CHZ.

The simulations demonstrate the important role played by the streamwise-oriented cells of helical motion in the entrainment of sediment particles from the bed and their downstream transport at confluences between non-parallel streams, regardless of the value of the momentum ratio. When the momentum ratio is close to one, the primary streamwise vorticies (SVs) are of comparable strength (some differences are induced by the asymmetry of the confluence and the relatively high curvature of the river reach downstream of the confluence), whereas when the momentum ratio is much larger than one, the SVs on the high momentum side of the ML are much stronger than the ones on the low-momentum side.

Analysis of the distributions of the bed friction velocity shows that if the momentum ratio is close to unity, the SVs developing on both sides of the ML are the main eddies responsible for the formation of the scour hole. As the momentum ratio between the two streams increases, the scour is mainly driven by the primary SV forming on the high momentum side of the confluence and by the eddies shed in the ML. The ML eddies are much more coherent than those observed in the case with Mr ≈ 1. When the momentum ratio is close to unity, the eddies convected within the mixing layer are similar to those forming downstream of a bluff body –von Karman vortex street- (wake type), whereas when the momentum ratio is much larger than one, the formation of the quasi 2D eddies is primarily driven by the velocity differential between the two streams, which drives the growth of Kelvin-Helmholtz instabilities (vortex sheet type). The second type of mechanism can generate much stronger ML eddies than the first type. The simulation results are consistent with findings from field investigations, which have suggested that ML turbulent structure is related to hydrodynamic conditions at the confluence apex (Rhoads and Sukhodolov, 2008).

REFERENCES

Boyer, C., Roy, A. G., Best, J. L. 2006. Dynamics of a river channel confluence with discordant beds: Flow turbulence, bed load sediment transport, and bed morphology, *J. Geophys. Res.*, 111, F04007.

Chang, K., Constantinescu, G., Park, S.O. 2007. Assessment of predictive capabilities of Detached Eddy Simulation to simulate flow and mass transport past open cavities. ASME J. Fluids Engineering, 129(11), 1372-1383.

Chu, V. H., Wu, J. H., and Khayat, R. E. 1991. Stability of transverse shear flows in shallow open channels. *J. Hydraul. Eng.*, 117 (10), 1370-1386.

Kenworthy, S.T. and Rhoads, B.L. 1995 Hydrologic control of spatial pattern of suspended sediment concentration at a small stream confluence. J. Hydrology, 168, 251-263.

Kirkil, G., Constantinescu, G. 2009. Nature of flow and turbulence structure around an in-stream vertical plate in a shallow channel and the implications for sediment erosion. Water Resources Research, 45, W06412, doi:10.1029/2008WR007363.

Koken, M., Constantinescu, G. 2009. An investigation of the dynamics of coherent structures in a turbulent channel flow with a vertical sidewall obstruction. Physics of Fluids, 21, 085104, DOI 10.1063/1.3207859.

Mosley, M. P. 1976. An experimental study of channel confluences. *J. Geology*, 84, 535-562.

Miyawaki, S. 2009. Numerical investigation of scalar transport at a river confluence. CD-ROM Proceedings of the 33rd I.A.H.R. congress, Vancouver.

Miyawaki, S., Constantinescu, G., Kirkil, G., Rhoads, B. L., and Sukhodolov, A. N. 2009. Numerical investigation of three-dimensional flow structure at a river confluence. Proc., 33rd I.A.H.R. congress, Vancouver, Canada.

Paola, C. 1997 When streams collide. *Nature*, 387, 232-233.

Rhoads, B.L., and Kenworthy, S.T., 1995. Flow structure at an asymmetrical stream confluence. *Geomorphology,* 11, 273-293.

Rhoads, B. L. 1996. Mean structure of transport-effective flows at an asymmetrical confluence when the main stream is dominant. Coherent flow structures in open channels. John Wiley & Sons Ltd., 491-517.

Rhoads, B. L. and Sukhodolov, A. N. 2001. Field investigation of three-dimensional flow structure at stream confluences: 1. Thermal mixing and time-averaged velocities. *Water Resour. Res.*, 37 (9), 2411-2424.

Rhoads and Sukhodolov, 2004. Spatial and temporal structure of shear layer turbulence at a river confluence. *Water Resour. Res.*, 40, W06304.

Rhoads, B. L., Sukhodolov, A. N. 2008. Lateral momentum flux and spatial evolution of flow within a confluence mixing interface. *Water Resour. Res.*, 44, WR08440; doi:10.1029/2007WR006634.

Sukhdolov and Rhoads 2001. Field investigation of three-dimensional flow structure at stream confluences. *Water Resour. Res.*, 37, 2393-2410.

Uijttewaal, W. S. J. and Booij, R. 2000. Effects of shallowness on the development of free-surface mixing layers. *Physics of Fluids*, 12 (2), 392-402.

Zeng, J., Constantinescu, S. G., Blanckaert., K., and Weber, L. 2008. Flow and bathymetry in sharp open-channel bends: Experiments and predictions. *Water Resour. Res.*, 44 (9), W09401, 1-22.